

On the nature of regional seismic phases—II. On the influence of structural barriers

T. Furumura* and B. L. N. Kennett

Research School of Earth Sciences, Australian National University, Canberra ACT 0200, Australia

Accepted 1996 June 12. Received 1996 May 10; in original form 1996 February 1

SUMMARY

The blockage of the *Lg* wave by crustal barriers such as continental margins and graben structures has long been recognized as providing a very useful tool for mapping large-scale lateral crustal variations along the propagation path. Numerical simulation of *Lg*-wave propagation in complex anelastic media using the pseudospectral method provides insight into the nature of the propagation process using both snapshots of the wavefield and synthetic seismograms. A variety of 2-D structures have been investigated, including the influence of sediments, crustal thickness and attenuation.

Thick sedimentary basins covering a graben structure can have a major influence, since they remove *Lg* energy by generating *P* conversion and scattering—the principal mechanisms for strong *Lg* attenuation across a graben. The reduction of the *Lg* energy is reinforced by anelastic attenuation in the sediments as well as the influence of the gradually thinning crustal waveguide associated with an elevated Moho.

The extinction of *Lg* in a sequence of explosions fired across the central graben of the North Sea can be simulated by numerical calculations for the structure derived from refraction experiments.

Key words: lateral heterogeneity, *Lg* wave, Moho discontinuity, North Sea Central Graben, nuclear explosions, seismic modelling, synthetic seismograms, wave propagation.

1 INTRODUCTION

A dominant feature of the seismic wavefield at regional distances is usually the *Lg* phase representing the superposition of multiple *S*-wave reflections propagating within the crustal waveguide. The *Lg* wave produced by the *S*-wave radiation from a source can be efficiently trapped within the crustal waveguide to propagate long distances, because of perfect reflection at both the surface and the crust–mantle boundary for *S* waves with low phase velocity. The amplitudes of the crustal phases such as *Pg* and *Sg*, the mantle phases *Pn* and *Sn* and the surface wave *Rg* are quite sensitive to source depth and mechanism. However, the amplitudes of *Lg* waves are relatively insensitive to the *S*-wave radiation of double-couple sources for sources at any depth in the crystalline crust. As a result, *Lg* has often been used for robust magnitude measurements (e.g. Nuttli 1980), and in nuclear discrimination studies (see e.g. Pomeroy, Best & McEvelly 1982). Other applications include the estimation of crustal velocity gradients (e.g. Bowman & Kennett 1991) and crustal attenuation factors (e.g. Campillo 1987).

It has also long been recognized that the amplitude of the *Lg* phase is very sensitive to variations in the crustal structure along the propagation path. A number of studies have utilized this sensitivity of the *Lg* phase to map structural variations using anomalous propagation paths. The many tectonic regions studied include the Tibetan Plateau (e.g. Ruzaiкин *et al.* 1977; Ni & Barazangi 1983), central Asia (e.g. Kadinsky-Cade *et al.* 1981) and the western Alps (Campillo *et al.* 1993). Such studies display a clear outline of crustal heterogeneity by mapping the paths with poor *Lg* propagation across the region.

The amplitude of *Lg* is also well known to be very sensitive to the influence of continental–oceanic transition zones, where as little as 100 km of oceanic path is sufficient to block the transmission of the *Lg* wave (Press & Ewing 1952). The blockage of the *Lg* wave in continental shelf regions has also been reported for many regions, such as the North Sea (Gregersen 1984; Kennett & Mykkeltveit 1984) and the Caspian Sea (Maupin 1989). Kennett *et al.* (1985) showed a clear outline of the graben structure in the centre of the North Sea basin in a detailed map of the apparent crustal heterogeneity derived from many different *Lg* propagation paths across the North Sea.

Several attempts to understand the seismic disturbances of the *Lg* wave in such a graben zone have been made. Studies by

* Present address: Hokkaido University of Education, Midorigaoka 2-34-1, Iwamizawa, 068, Japan.

Kennett & Mykkeltveit (1984) using a higher-mode surface-wave summation technique and ray-theoretical approaches (Kennett 1986; Bostock & Kennett 1990) suggest that energy coupling between Lg modes and Sn modes associated with the elevation of the crust–mantle boundary beneath the graben zone is a major contributor to the attenuation of the Lg wave. Maupin (1989), however, using a coupled local-mode method, claimed that the strong Lg attenuation across the graben zone could not be fully explained by the thinning of the crust.

Numerical simulation of seismic wave propagation in complex media can provide a direct insight into the character of the wavefield and the propagation process through the use of a sequence of snapshots of the wavefield in time and space. Such studies of regional wave blockage have been made recently using an acoustic finite-element method (Regan & Harkrider 1989) and an elastic finite-difference method (Cao & Muirhead 1993). Regan & Harkrider (1989) used a 2-D model for an SH wavefield and suggested that the energy escaping from the slope of the crust–mantle boundary can cause severe attenuation of the Lg wave. These results are supported by the work of Cao & Muirhead (1993), who demonstrated that the existence of the water-column and topographical variations can be very important factors in severe Lg attenuation. However, Zhang & Lay (1995) claimed that the thinning crust plays a more important role in breaking up the Lg packet than the effects of the change of the crustal thickness itself.

Unfortunately, the previous results are based on completely different models and use different wave types, and so cannot be readily compared. It is therefore difficult to judge the relative importance of different aspects of the variations in crustal properties on the blockage of the Lg phase. Moreover, most of the modelling has been undertaken with perfectly elastic media and so ignores the influence of high intrinsic attenuation in near-surface sediments on the regional wavefield.

The object of this paper is to investigate the nature of the disturbance in the seismic wavefield at regional distances produced by crustal barriers. We will make use of the 2-D pseudospectral method (see e.g. Furumura & Takenaka 1996) to calculate the seismic wavefield in a 2-D anelastic model as a means of investigating the relative importance of different aspects of crustal structure across a graben-like feature for the

blockage of the Lg wave. Sequences of snapshots with the seismic wavefield separated into P , SV and SH components demonstrate the dynamic propagation processes as the waves interact with crustal barriers.

We first demonstrate the prominence of the Lg phase generated by a double-couple line source, propagating within the crustal waveguide in a shield structure. This same base model is then combined with different styles of crustal barriers to investigate the nature of the interactions of the regional wavefield with the lateral heterogeneity. A simple graben model produces significant Lg attenuation, and by changing various aspects of the model we are able to compare the influence of different classes of structure using both snapshots of the wavefield and synthetic seismograms. We examine the relative importance of crustal variations, due to crustal thinning with elevation of the Moho and the presence of thick sediments, on the blockage of the Lg propagation. Finally, we simulate the change in Lg -wave propagation characteristics across the North Sea Central Graben region in order to complement the observations described by Kennett & Mykkeltveit (1984).

2 Lg BLOCKAGE BY CRUSTAL BARRIERS

We use the pseudospectral method to provide numerical simulations of seismic wave propagation in anelastic 2-D models for both P – SV and SH wavefields. This alternative attractive finite-difference modelling scheme (Furumura & Takenaka 1996) is very efficient for large-scale modelling because it offers high-accuracy results with substantially less computation time and memory than traditional schemes.

As a first example we compare the propagation of regional seismic phases in a shield structure and a simple model of a graben. We use a double-couple source in the shield structure in each case, and then compare a sequence of wavefield snapshots for P , SV and SH components, as well as synthetic seismograms for vertical, radial and transverse components of motion. These comparisons indicate a significant reduction of the Lg phase in transmission across the graben.

The model we use here is schematically illustrated in Fig. 1; it is similar to that employed by Kennett & Mykkeltveit (1984) and Cao & Muirhead (1993), in which a crustal pinch

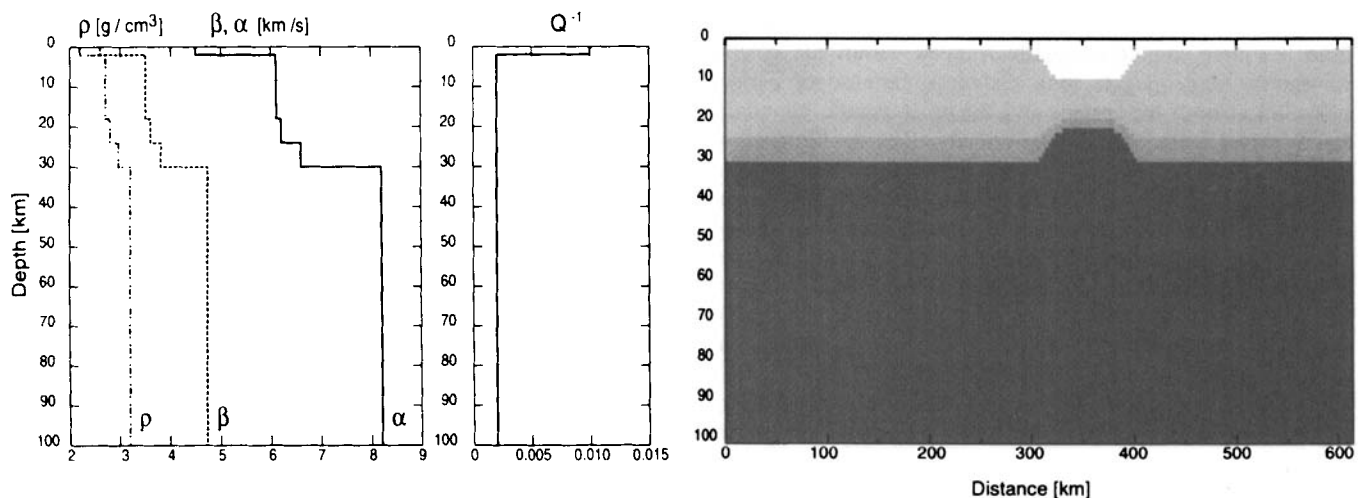


Figure 1. The depth variation of P (α)- and S (β)-wave velocities, density (ρ) and the loss factor (Q^{-1}) used in the 2-D numerical modelling, illustrating the shield reference structure and the simple graben model.

associated with an elevation of the Moho and thick sediments in the centre of the model represent a simple graben structure. The numerical models for the shield and the graben structure both cover a zone 614.4 km long by 153.6 km deep with a regular grid interval of 1.2 km. In the pseudospectral method just two grid points per wavelength are theoretically sufficient to treat the seismic wave propagation, and therefore the shortest wavelength appearing in the modelling is 2.4 km. The influence of the grid-edge effects on the display domain is minimized by use of a suitable absorbing buffer zone (Cerjan *et al.* 1985) surrounding the region.

We have used a rather deep line source ($H = 20.4$ km) with double-couple radiation for the P - SV field and a single force for the SH field, with a source-time function of a pseudo-delta function which imparts a predominant frequency of 1 Hz. The advantage of using a deep source is that it produces a large Lg phase while the fundamental Rayleigh Rg wave is weakened. Thus we can concentrate on the influence of crustal barriers on the Lg wave without interference from the Rg phase.

We present a sequence of snapshots of the wavefield separated into P , SV and SH components, superimposed on the structural model, which gives us a direct insight into the characteristics of the wave propagation including the influence of conversions between P and SV waves produced at discontinuities. The P contribution is shown in black and the SV component in white. The sequence of snapshots for the P - SV wavefield in the undistorted shield model is illustrated in Fig. 2(a), with a regular time interval between frames, extending until the Lg phase approaches the edge of the frame. The change in the wavefield for the P and SV components produced by the presence of the lateral variations in the crustal structure in the simple graben model can be readily seen in Fig. 2(b) by a comparison with the corresponding snapshots for the reference wavefield in Fig. 2(a).

In the upper frame (14 s) of Figs 2(a) and (b) we see the radiation of P and S waves from the double-couple strike-slip-fault source, which produces large Pn and Pg phases (28 s). By the 42 s frame we can discern two Pn contributions, generated by direct downward P radiation and also upward P radiation from the source which is then reflected at the free surface. The strike-slip fault source radiates strong S energy into the crust, which leads to a prominent Lg phase build up from multiple SmS reflections in the crust. The Lg phase is already clear in the first few frames. The Rg phase for the deep source is very weak and cannot readily be seen in any of the snapshots.

In the middle (70 s) frame we can see that the Pg wave has been noticeably weakened by passage through the graben zone, while the Pn wave maintains its amplitude during transmission across the zone of crustal thinning. As the Lg phase approaches the sedimentary basin on the top of the graben structure, significant conversion to P occurs at the sloping sides of the sedimentary basin, which extracts energy from the Lg packet (84 s). In the 98 s frame we can discern some Lg energy escaping from the crustal waveguide into the mantle, which also weakens the S energy retained in the crust. Consequently, in the last few frames (126 s, 140 s, 154 s), we can see that the Lg phase has been significantly weakened by the influence of the lateral variation in crustal structure.

The strong influence of the graben structure on Lg is also seen in the SH wavefield displayed in Fig. 3. As in Fig. 2, the snapshots for the reference wavefield in the shield structure

are shown on the left and the corresponding time frames for the simple graben structure are shown on the right. The mantle S wavefront giving rise to the Sn phase has separated out very clearly by the 42 s frame. Sn is a prominent feature of the wavefield in all of the frames, and is somewhat larger than for the P - SV wavefield in Fig. 2 because the radiation pattern for the single force enhances S -wave energy propagating diagonally towards the mantle-crust boundary, which then efficiently produces the Sn phases. In contrast, the amplitude of Lg is reduced compared to Fig. 2 because the radiation is less favourable for multiple SmS reflections.

However, in the last three time frames (126 s, 144 s, 154 s) there is still a distinct Lg packet in the reference wavefield (Fig. 3a), but it is much weaker after transmission through the simple graben structure (Fig. 3b). It is interesting to note that the attenuation of the Lg wave for the SH component is not as dramatic as for the SV component, where there can be conversion from Lg energy into P waves.

The attenuation of the regional phases by the lateral variations in the crustal structure is also clearly demonstrated by comparing the synthetic seismograms of the vertical, radial and transverse (SH) components of ground velocity at the free surface for the reference shield structure and the simple graben model (Fig. 4). In the seismograms we can discern the Pn phase as a first arrival on the vertical and radial components with a group velocity of 8.2 km s^{-1} , and the Sn wave with a group velocity of 4.8 km s^{-1} and significant amplitude on the transverse component. Neither of these mantle phases is strongly affected by the presence of the crustal variations.

The Pg train appears in the seismograms with a group velocity of 6.0 km s^{-1} on the vertical and radial components. In the presence of the graben, Pg is disrupted by interaction with the left-hand side of the graben structure and cannot be tracked beyond about 350 km. The Lg wave appears on all three components with a group velocity of 3.5 km s^{-1} , and the regular pattern of multiple SmS reflections can be clearly seen for the reference structure (Fig. 4a). For the graben model (Fig. 4b), the Lg wave is amplified by the sediments on the top of the graben for distances around 320 km, and the regular reflection pattern is disrupted by the presence of the graben so that Lg is severely diminished in amplitude beyond 350 km.

The reduction in amplitude of the Lg phase produced by this simple graben model is about 1/2 for the vertical component, 1/4 for the radial components, and 1/3 for the transverse (SH) component. These attenuation factors agree fairly well with previous studies (e.g. Maupin 1989; Cao & Muirhead 1993).

3 Lg ATTENUATION DUE TO VARIATIONS IN CRUSTAL STRUCTURE

In order to try to understand the change in the character of the Lg wave effected by different crustal barriers, we have made a series of numerical simulations using three models that include part of the crustal variations making up a realistic graben model. The first model has only a thinning of the crust produced by an elevation of the Moho. The second model includes the effect of a thick sedimentary sequence at the surface. The third model has a water layer over the graben structure.

We show a sequence of snapshots and synthetic seismograms for the P - SV wavefield rather than for the SH wavefield, because the Lg attenuation on the vertical and radial

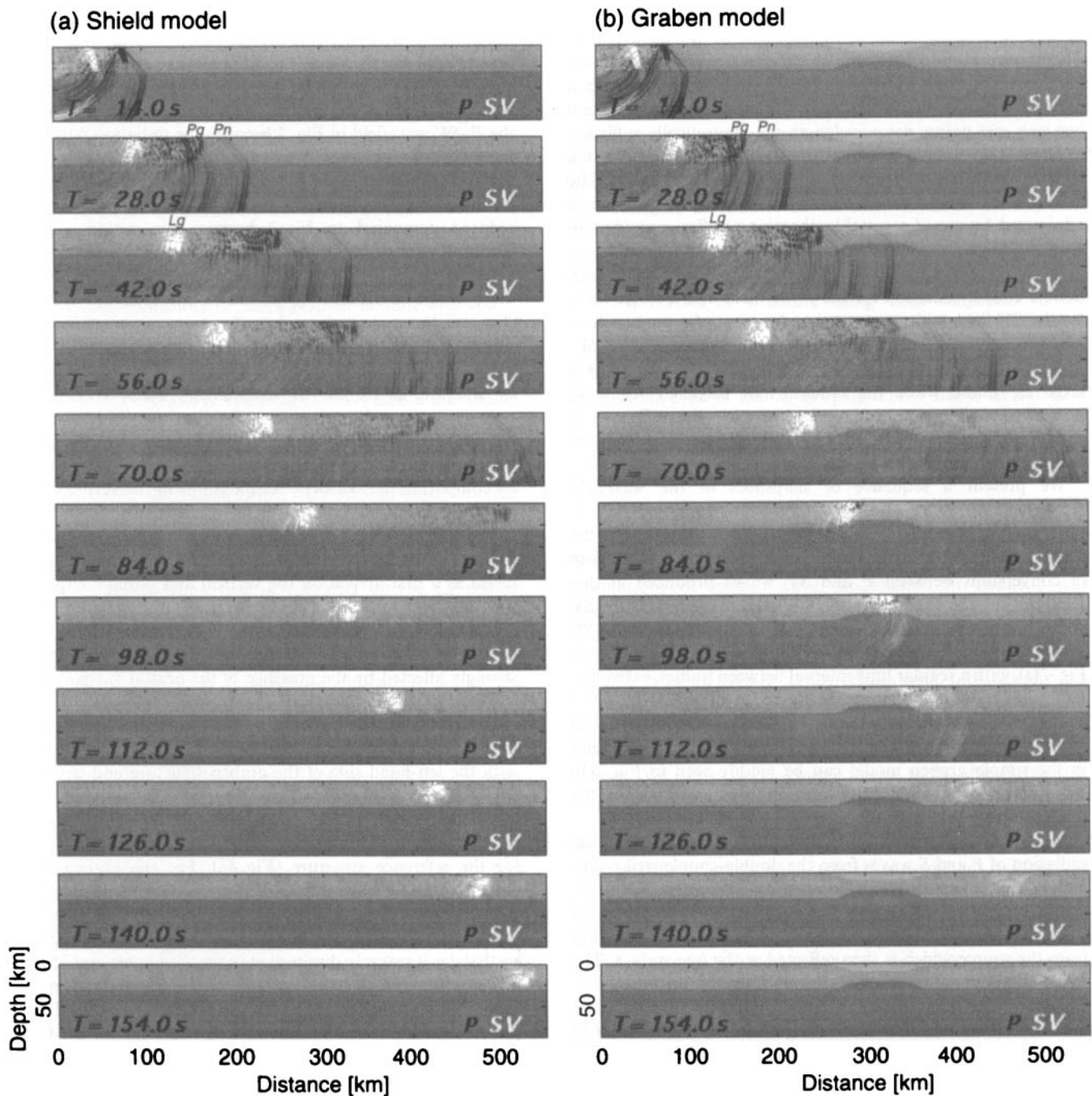


Figure 2. Snapshots of the seismic wavefield illustrating the P and SV components of the wavefield as functions of distance from the source and time; the P -wave contribution is shown in black and the S -wave contribution in white. A double-couple source is placed 20 km below the free surface: (a) for the shield model; (b) for the simple graben model.

components that is associated with conversions between Lg and P is more severe for the vertical and radial components than for the transverse component.

3.1 Effect of mantle uplift

The first calculation is just for the effect of a crustal pinch, with crustal thinning produced by raising the Moho from 30 km to nearly 20.4 km depth over the distance range of 260 to 370 km. This crustal pinch is accompanied by strong horizontal gradients in the velocity structure.

A sequence of wavefield snapshots and seismograms of vertical and radial velocity components for the model are displayed in Fig. 5(a) with the same amplification factor as in the previous illustrations. In the 84 s time-frame we can discern some Lg energy leaking into the mantle by refraction through the slope of the crustal pinch. The Lg -wave energy is concentrated as it passes through the thinner waveguide, and relatively large P conversions occur at the base of the near-surface sediments (98 s). Moreover, the SV multiple reflections are also distorted by scattering at the far edge of the Moho uplift, which then leads to an elongation of the Lg wave packet.

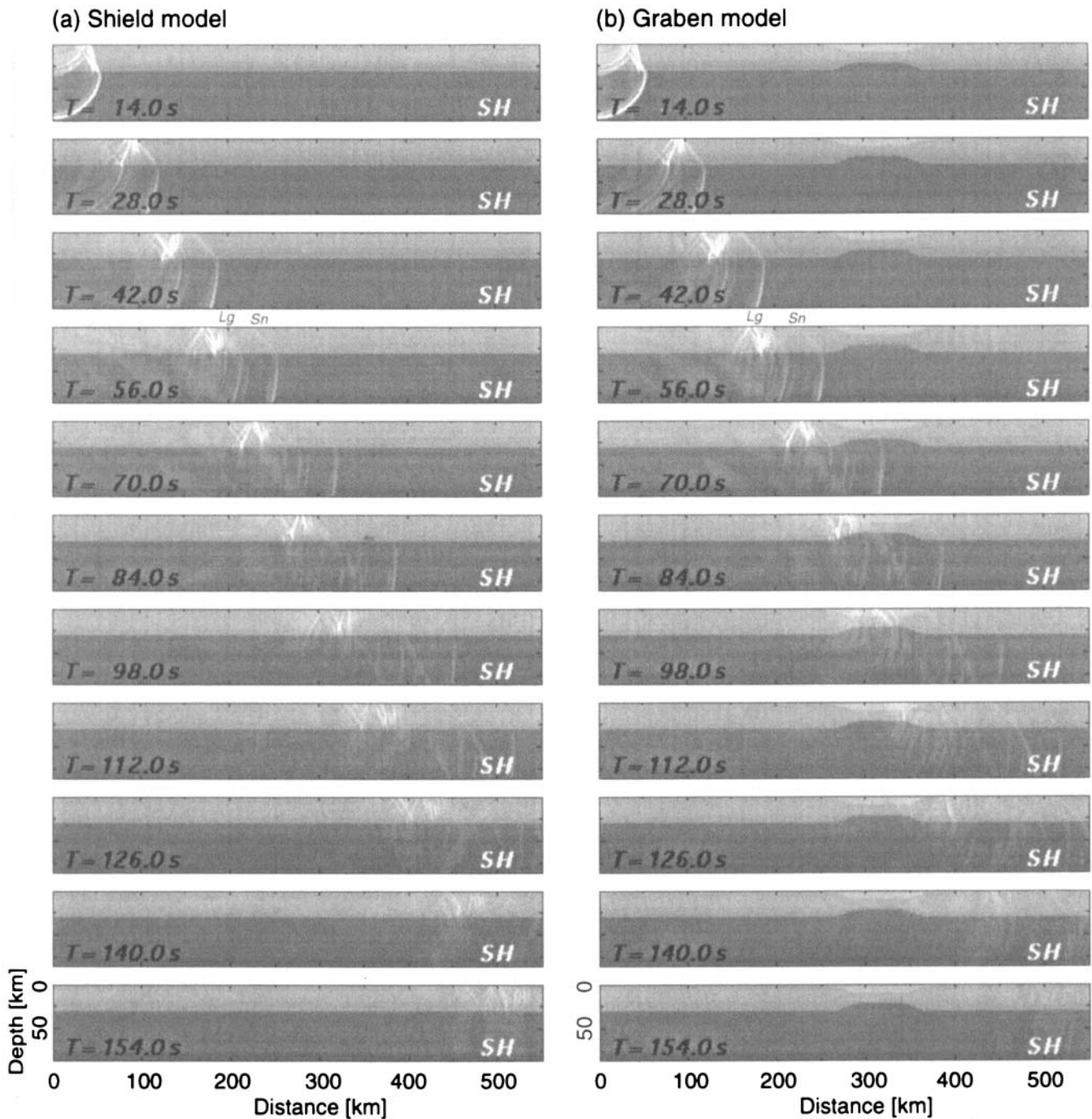


Figure 3. Snapshots of the seismic wavefield illustrating the *SH* components of the wavefield as functions of distance from the source and time. A directional *SH* source is placed 20 km below the free surface: (a) for the shield model; (b) for the simple graben model.

For this model, however, the loss of energy associated with scattering and energy escaping from the crust, as it thins, is small compared to the total *Lg* energy passing through the thin waveguide. The reduction of the *Lg* amplitude by this class of crustal barrier is at most 2/3 compared with the shield reference model. This effect is insufficient to explain the severe *Lg* attenuation for the previous full graben model.

In order to confirm the influence of a Moho uplift on the blocking of the regional phases we have performed another calculation for an extreme Moho model in which the Moho depth is suddenly changed from 30 km to 6 km (typical for

oceanic crust) over a 110 km zone. The seismograms and snapshots for this case are illustrated in Fig. 5(b). For this model, the *Pg* wave is considerably weakened (see the 84 s frame), while the *Lg* is reduced in amplitude but not eliminated. In the 98 s time-frame we see significant *Lg* energy escaping into the uppermost mantle from the Moho pinch, and at 128 s there are large *Pg* conversions, produced from the slope as the Moho returns to its original depth, which also remove the *S*-wave energy from the *Lg* wave. In this 128 s frame we can also see the separation of a mantle *S* wavefront, giving rise to a secondary *Sn* wave which is found in the synthetic

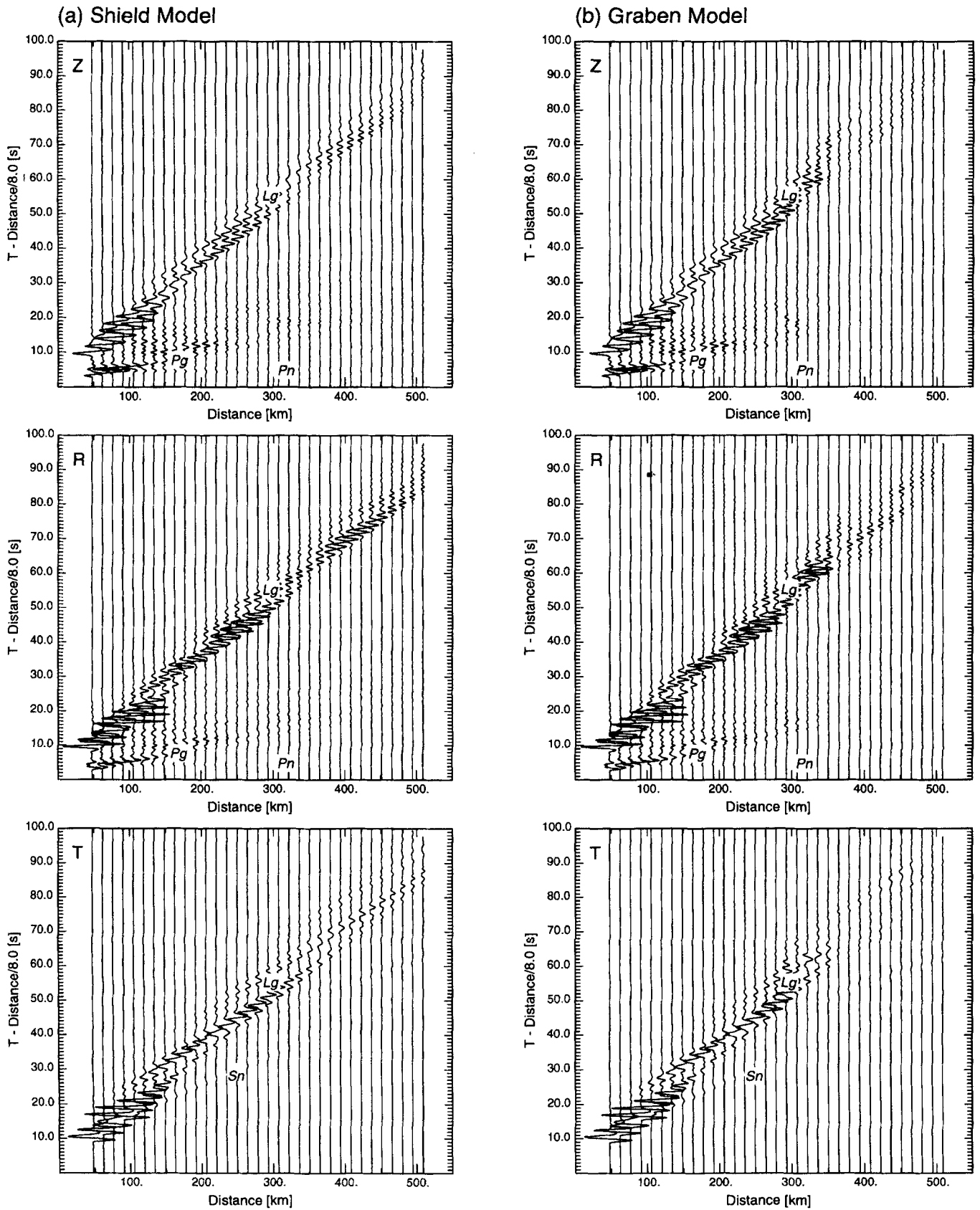


Figure 4. Synthetic velocity seismograms for both vertical (Z) and radial (R) components calculated by *P-SV* pseudospectral modelling, and transverse components (T) calculated by *SH* modelling: (a) for the shield model; (b) for the simple graben model.

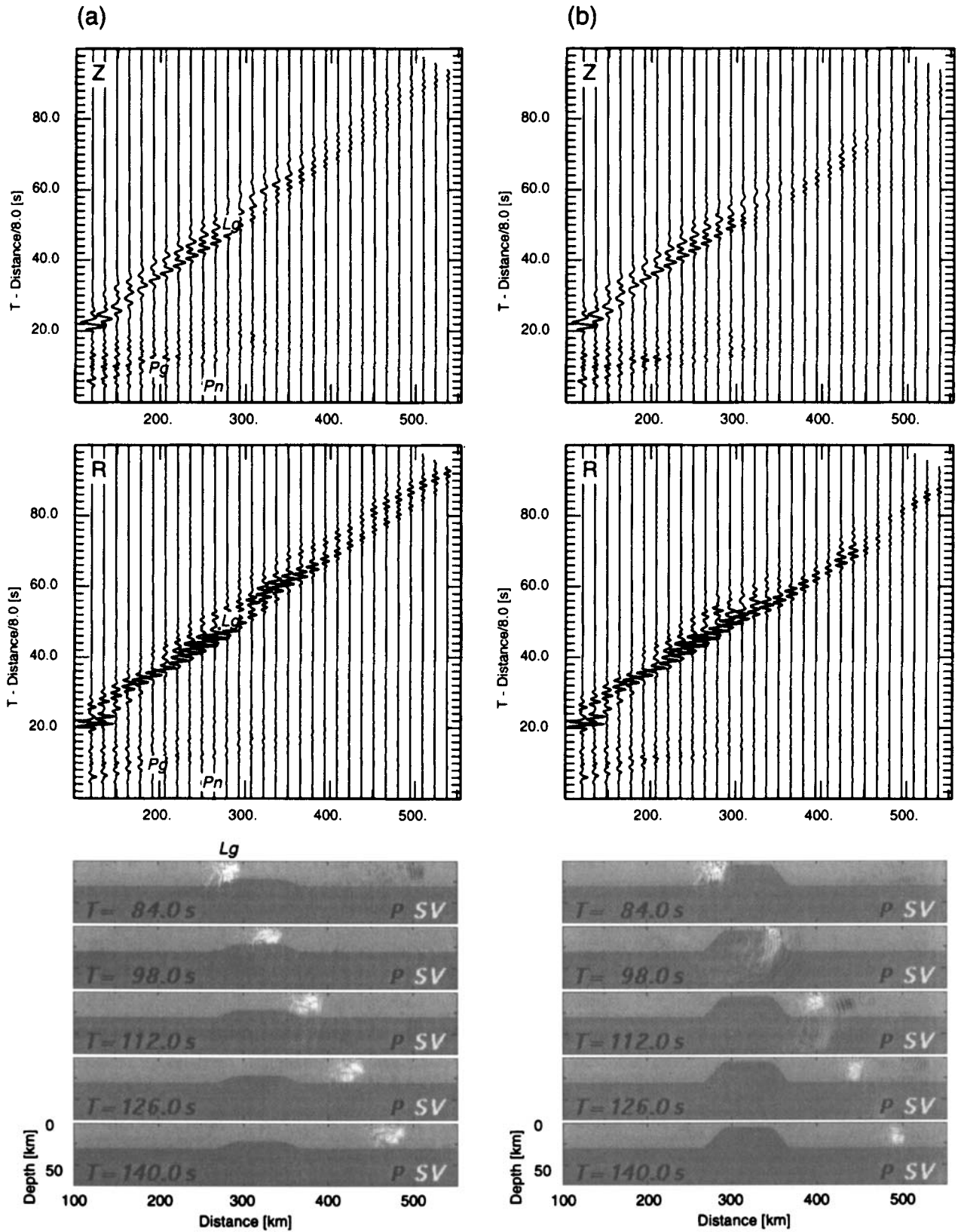


Figure 5. Synthetic velocity seismogram for both vertical (Z) and radial (R) components and snapshots of the seismic wavefield illustrating the P and SV components of the wavefield: (a) Moho uplift; (b) extreme Moho uplift.

seismograms of both vertical and radial components at distances between 300 and 400 km. However, it is very interesting to note that, even with the very thin crust of 6 km thickness, there can be relatively efficient transmission of the radial component of Lg even though there is a noticeable change in the pattern of multiple S reflections. This is produced in part by the reinforcement of the Lg wave, which has passed through the thin crust by means of the S wave transmitted through the uppermost mantle beneath the zone of crustal thinning (112 s).

In consequence we can state clearly that the influence of crustal thinning alone cannot explain the severe Lg attenuation seen across graben structures.

3.2 Effect of sedimentary basins

The Lg attenuation produced by a sedimentary basin is considered in a model which includes thick sediments with a lower velocity ($\alpha = 4.5 \text{ km s}^{-1}$, $\beta = 2.6 \text{ km s}^{-1}$) and higher attenuation ($Q = 100$) than the crystalline crust but without a change in the overall crustal thickness. The basin is 7 km deep and 100 km long. Snapshots of the wavefield and the seismograms for the basin model are displayed in Fig. 6(a) with the same amplification factors as for the previous examples.

In the 84 s time-frame we notice P conversions from Lg generated at the edge of the basin, which then continue to propagate as a secondary Pg wave. The influence of the sedimentary basin modifies the propagation characteristics of the S energy in the crust and leads to some radiation into the mantle, which can be seen in the 98 s frame. Part of the crustal S energy is spread out by multiple reflection and scattering, leading to an elongation of the Lg wave-packet as can be seen in the synthetic seismograms. The slower velocity of the waves in the sediments tends to reduce the group velocity slightly compared with the reference model.

The portion of the Lg energy propagating in the basin is also noticeably reduced by intrinsic attenuation and scattering by the sediment (see the time-frames for 98 s and 112 s). The importance of such attenuation is confirmed by comparing the seismograms with those for a perfectly elastic model, which shows only a slight decrease of the rate of decay (about 1/2 of the anelastic model) of the Lg produced by the presence of a sedimentary basin.

The synthetic seismograms for the vertical and radial components calculated for this sedimentary basin model are illustrated in Fig. 6(a). There is a temporary amplification of the Lg energy over the sediment zone beyond 280 km but the amplitudes diminish beyond 350 km.

The reduction in Lg amplitude for this sedimentary basin model is at most about 1/3, which is insufficient to explain the strong loss for the full graben model (to about 1/4 of the original amplitude—see Figs 2 and 4).

The attenuation of the Lg phase is more pronounced for larger sedimentary basin structures, both where the basin contains thicker sediments (Fig. 6b—14.4 km of sediments) and where the same thickness is sustained for a longer distance (Fig. 6c—160 km long basin). Snapshots and synthetic seismograms are displayed on the same scale as Fig. 6(a) and indicate the significant weakening of the Lg phase after transmission through the models containing these larger basins. Conversion to P energy is more pronounced than for Fig. 6(a), and the longer passage in the zone of lower Q extracts energy from the crustal S wavefield.

A thick sedimentary basin can therefore induce significant energy loss for Lg , which can help to reinforce the losses caused by disruption of the wavefield in a zone of crustal thinning. The strong influence of a very thick sedimentary layer is in good agreement with the observations of Baumgardt (1990) of Lg blockage on paths from Novaya Zemlya to NORESS and ARCESS crossing the Barents Sea. The south Barents Sea basin has a layer of sediments over 10 km thick associated with crustal thinning of nearly 10 km.

3.3 Effect of water coverage

Where water overlies a sedimentary basin, additional attenuation can be expected because conversion into P waves in the water can extract further energy from the S wavefield. The effects are illustrated for a graben model in which a layer of water lies on top of the sediments. The model has a water thickness of 1.8 km and a width of 110 km, with a P -wave velocity of 1.5 km s^{-1} , a density of 1.0 g cm^{-3} and an anelastic attenuation factor of $Q = 1000$. Since the minimum wavelength in this low-velocity zone (1.5 km) is somewhat shorter than in the earlier calculations (2.4 km), we used a smaller grid spacing of 0.6 km to avoid aliasing errors. As a result, care is needed when comparing the snapshots and synthetic seismograms with those in the previous figures, because the wavefield is dominated by much higher frequencies than before.

The snapshots of the wavefield and the synthetic seismograms for the model are displayed in Fig. 6(d). In the first few frames (84 s, 98 s, 112 s) we see very strong scattering into the crust produced at the edge of the water zone. The influence of the water coverage on the wavefield can be seen by comparison with Figs 2 and 4. There are strong P conversions in the water and sediments, accompanied by scattering effects at the edges of the basins. Consequently, the Lg wave can be drastically weakened by passing through a sedimentary basin with superimposed water coverage.

4 Lg BLOCKAGE IN THE NORTH SEA CENTRAL GRABEN

In this section we will attempt to understand the nature of the Lg waves produced by an explosive source fired at the free surface, and the process of Lg extinction after passage across the Central Graben zone of the North Sea. Kennett & Mykkeltveit (1984) have presented a set of seismograms recorded at the NORSAR seismic array from a line of explosions in which Lg waves are clearly seen for shots on the northeastern (Norwegian) side of the Central Graben, but where the explosions on the southwestern (British) side of the graben have no distinct Lg arrivals. A number of attempts have been made to understand the mechanism of such Lg attenuation by the graben zone—modal-coupling methods at fixed frequency were used by Kennett & Mykkeltveit (1984) and Maupin (1989), whilst Cao & Muirhead (1993) used an elastic finite-difference scheme for a simplified graben model. In each case it has proved possible to explain part of the attenuation, but the dramatic loss of Lg energy has not been reproduced.

Here we model the seismic wavefield including anelastic attenuation for the 2-D model of the North Sea Central Graben region, which was obtained by Wood & Barton (1983) from the interpretation of a major seismic refraction experiment. Since the main trend of the structural features in the

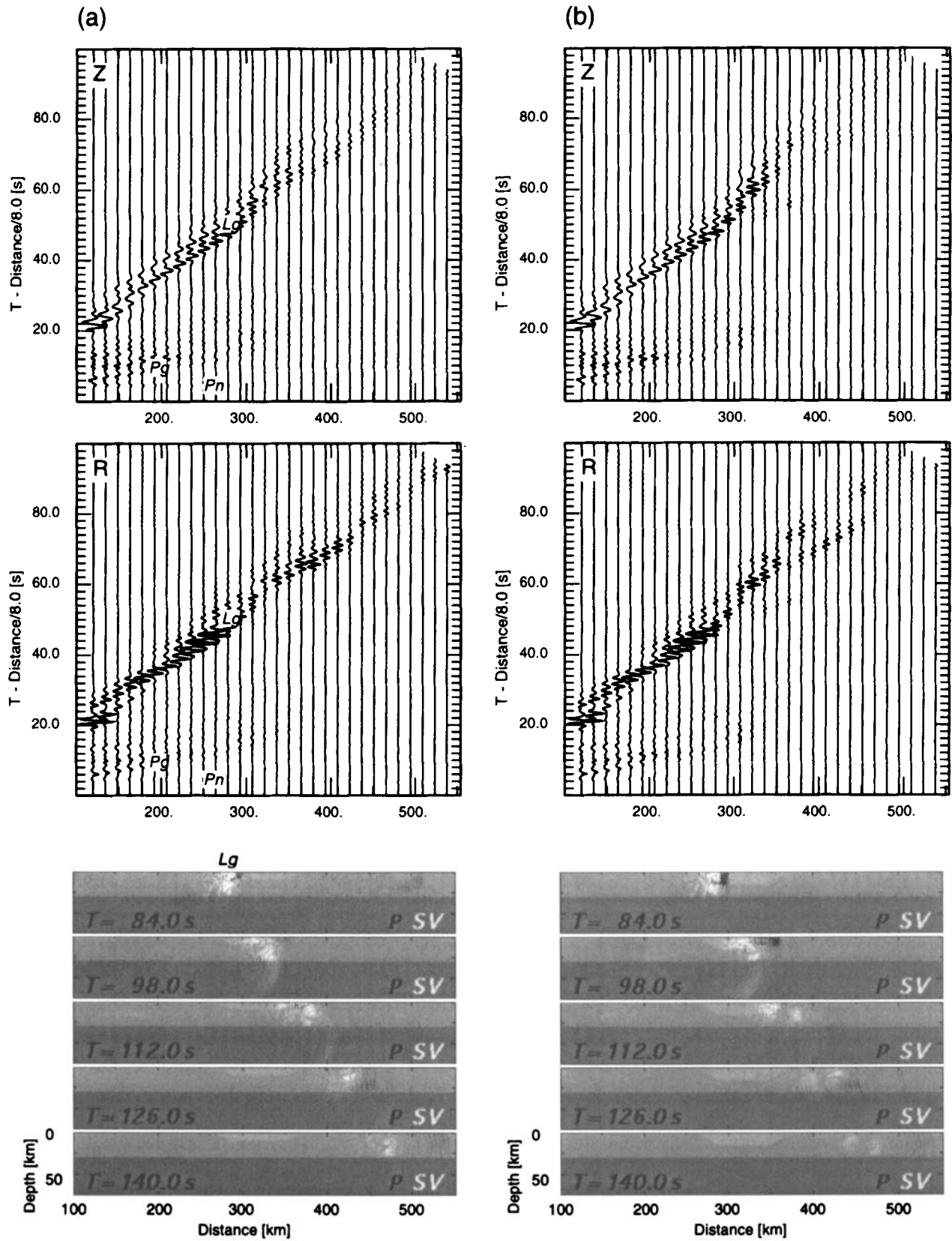


Figure 6. Synthetic velocity seismogram for both vertical (Z) and radial (R) components and snapshots of the seismic wavefield illustrating the P and SV components of the wavefield: (a) sediment model; (b) thick sediment model; (c) long sediment model, (d) graben with water-column in the basin model.

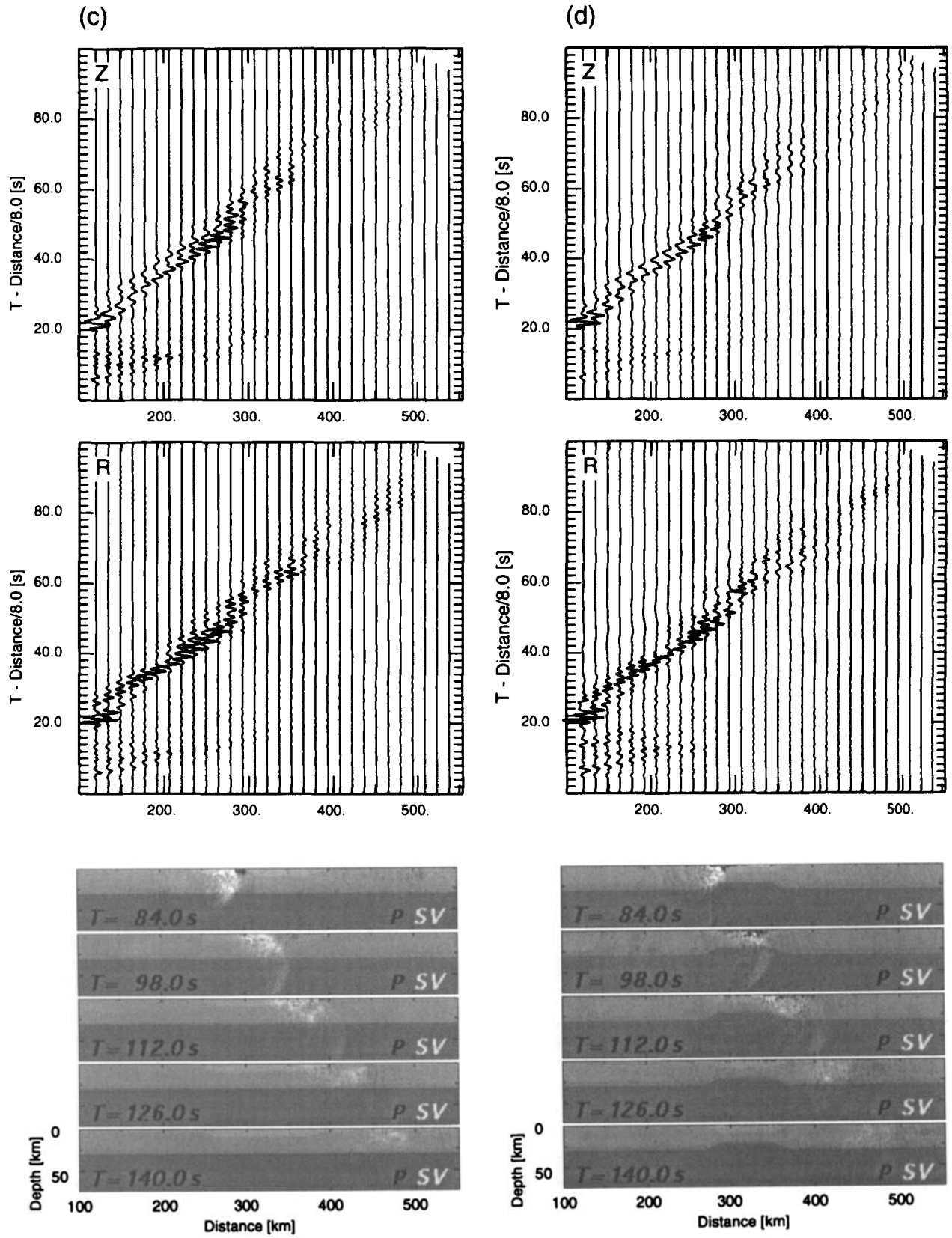


Figure 6. (Continued.)

North Sea Central Graben is almost close to perpendicular to the paths to NORSAR, we are able to use the 2-D model as a very good approximation to the actual situation. The model includes a thick sedimentary basin with a maximum thickness of 9 km at the centre of the graben, which extends for nearly 300 km with sediment thinning to the northeast. The Moho is uplifted beneath the Central Graben, with associated strong lateral variations in seismic velocity. We have assumed an anelastic attenuation factor of $Q = 100$ for the sediments and of $Q = 500$ for the remainder of the model. We have excluded a water layer from the wavefield modelling because the water depth around the North Sea Central Graben is very shallow (<200 m) and therefore cannot be adequately represented with current computational resources when we consider propagation of regional phases for long distances. The neglect of the influence of the thin water layer should not have a significant effect on most aspects of the wavefield, but will mean that we will tend to underestimate Lg attenuation.

We will first look at the evolution of the regional wavefield as the waves propagate from an explosive source to impinge on the graben model. Then we will use the seismic reciprocal theorem to look at a set of explosions at different positions relative to the graben but recorded at a single site, which simulates the observations discussed by Kennett & Mykkeltveit (1984).

4.1 Lg transmission across the North Sea Central Graben

The graben model we have used is 665.6 km long by 83.2 km deep, represented by a 1024×128 grid with a regular grid interval of 0.65 km. An explosive source with a predominant frequency of 1 Hz is placed on the free surface at a distance of about 300 km from the centre of the graben. A sequence of snapshots for the P and SV components of the seismic wavefield is displayed in Fig. 7, with the same amplification factor for all the frames. The distance represents the range from the NORSAR seismic array, as in Kennett & Mykkeltveit (1984—Fig. 2).

In the first frame (3.5 s) we see the P wave radiating isotropically from the explosive source fired on the free surface, as well as the S wave generated by P -to- S conversion at the free surface. In the 14 s time-frame we find the Pn head wave separating from the Pg wave. This mantle arrival is not affected much by the changes in crustal structure (see 42 s and 56 s). In the 28 s frame the Pg wave has reached the edge of the sedimentary basin, with associated strong S conversion at the surface so that the part of the Pg field propagating in the sedimentary basin is severely weakened (see 56 s, 70 s).

By the 42 s frame we see a strong S wavefront, generated from energy converted from P at the free surface. S reflections at the crust–mantle boundary and the surface help to build up the Lg phase, which remains a prominent feature for the next few frames. In the middle set of frames (70 s, 84 s) we find that the slope of the Moho uplift has the effect of pushing energy from the Lg packet into the sediments, so that strong P conversions are produced at the free surface (see 70 s). The S wavefield passing through the zone of maximum thinning is considerably distorted by scattering and P -wave conversions, and in consequence the Lg wave is drastically weakened when crossing this part of the structure. The S -wave energy left in the crustal waveguide after the passage through the thin crust is very weak and diffuse, so the Lg packet cannot be rebuilt.

The fundamental Rayleigh wave Rg is very efficiently produced by the shallow source in the solid medium and is a

prominent feature throughout the frames. The Rg packet propagating along the free surface is gradually prolonged by dispersion in the sediments. In the 84 s frame we can see Rg energy escaping from the slope of the sedimentary basin; however, the maximum amplitude of the Rg phase is almost unchanged. The main influence of a thin water layer in a real situation would be to change the character of the Rg propagation by modifying the surface conditions.

Fig. 8 displays the synthetic seismograms of vertical and radial components of ground velocity, in which we can see the dominance of the Lg arrival on the radial component with a group velocity of 3.0 to 3.4 km s⁻¹, as well as the Rg wave on the vertical component with a group velocity of 2.7 to 2.9 km s⁻¹. After passing through the centre of the graben region, the crustal waves such as the Lg and the Pg waves are suddenly extinguished. The graben zone also changes the shape of the Rg phase, but its maximum amplitude is unchanged.

These numerical modelling results are consistent with the severe Lg attenuation observed for propagation across the North Sea Central Graben.

4.2 Lg blockage by the North Sea Central Graben

In order to complement the observational results of a significant change in the seismograms for the source around the North Sea Central Graben zone as described in Kennett & Mykkeltveit (1984), we perform numerical modelling of seismic wave propagation in the North Sea and severe Lg -wave extinction crossing the graben zone. We use the seismic reciprocal theorem to extract the seismograms of many sources at a time for a single receiver position.

We have extended the model employed in the previous section by the addition of a shield structure on the right-hand side of the model to extend the propagation into the NORSAR array. The overall dimensions of the model are then 1331.2 km long by 83.2 km deep. Each seismic source has the same characteristics as in the previous example.

Fig. 9 illustrates the seismograms of vertical and radial components of ground-velocity motion for the surface receiver and corresponds to many different explosion sources fired at the surface, with distances from the receiver ranging from 100 to 900 km. The distances are indicated from the fixed receiver so the aspect of the seismograms appears rather different from that in Fig. 8 with a fixed source and variable receivers.

For the closer sources, the Lg phase can be clearly seen on the vertical and radial components with a group velocity ranging from 3.1 to 3.4 km s⁻¹, and can be tracked back to about 625 km from the receiver. However, Lg suddenly disappears for the sources placed on the left-hand side of the graben zone, i.e. on the side farther from the receiver. The extinction of Lg for the ranges greater than 650 km is in very good agreement with the observations of Kennett & Mykkeltveit (1984—Fig. 2), where Lg was seen for shots up to 625 km from the array, but not for the next shot at 782 km on the British side of the graben.

The synthetic seismograms of Fig. 9 show that the Pg wave with a group velocity of about 6.2 km s⁻¹ is also extinguished for the sources placed on the southwestern side of the graben zone, whereas the mantle phases, Pn and Sn , can be seen clearly for all the shots and are not greatly affected by the presence of the crustal barrier.

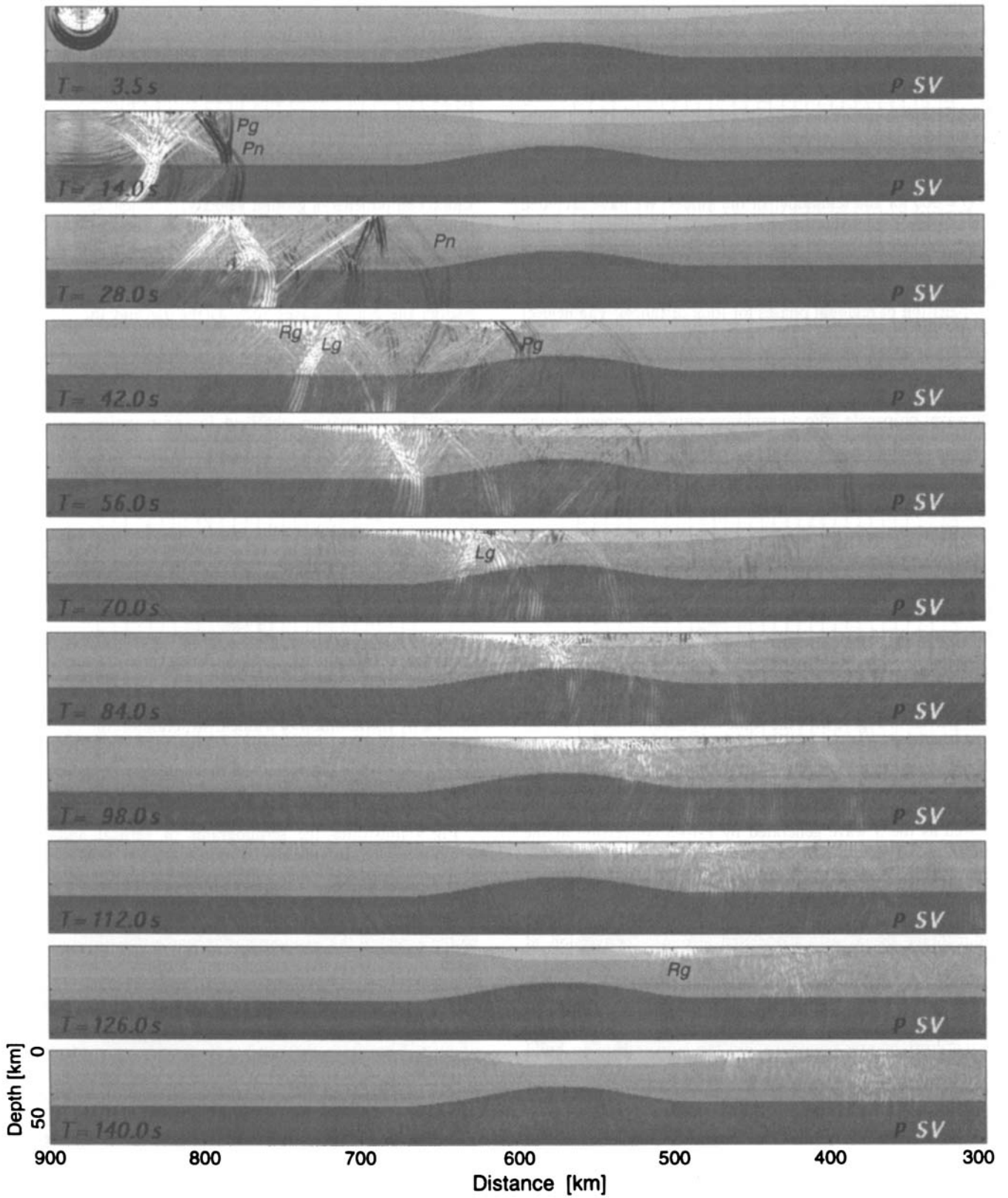


Figure 7. Snapshots of the seismic wavefield for the North Sea Central Graben model illustrating the P and SV components of the wavefield as a function of distance from the source and time; the P -wave contribution is shown in black and the S -wave contribution in white. An explosive source is placed at the surface.

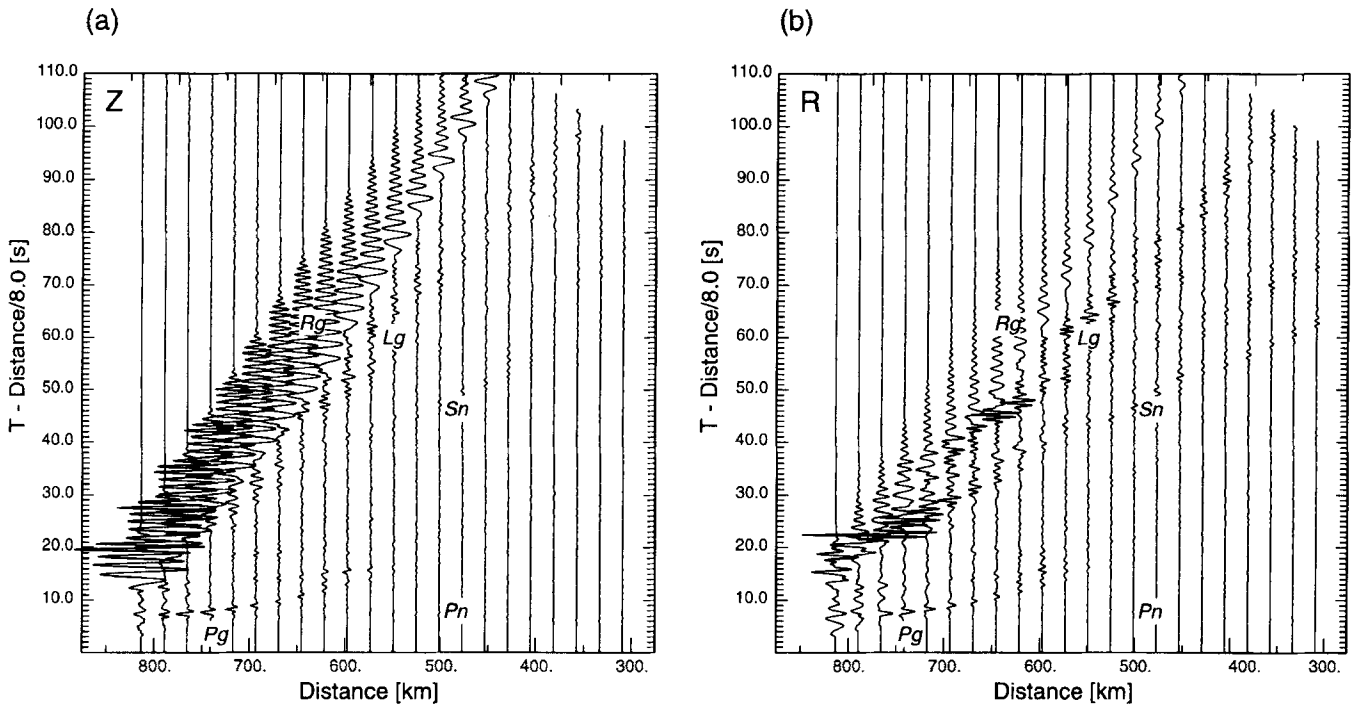


Figure 8. Synthetic velocity seismograms for the North Sea Central Graben model for both (a) vertical and (b) radial components calculated by *P-SV* pseudospectral modelling for a surface explosive source.

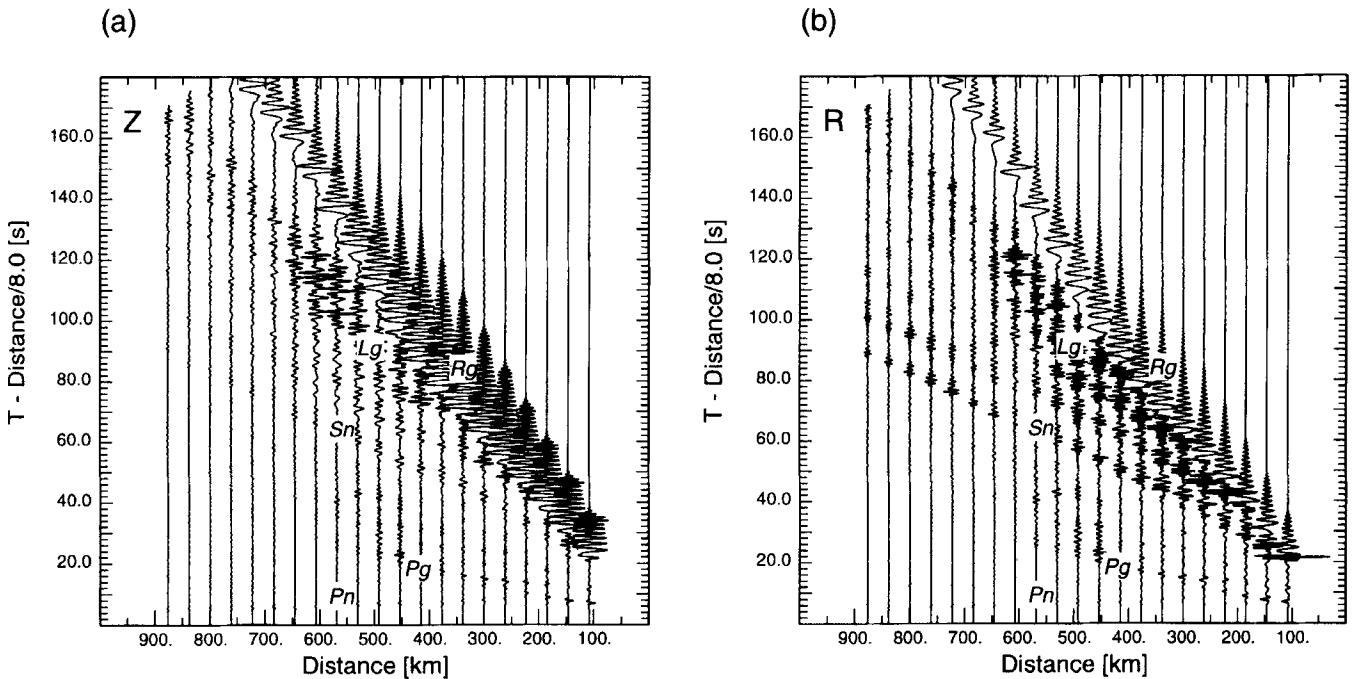


Figure 9. Synthetic velocity seismograms for the North Sea Central Graben model for both (a) vertical and (b) radial components of the receivers located on the NORSAR for many explosion sources fired at the surface, calculated by combining seismic reciprocity with *P-SV* pseudospectral modelling.

It is interesting to note that the thick sediment which contributes strongly to the blockage of the *Lg* wave for more distant sources is at the same time able to produce efficiently the *Lg* wave from explosion sources fired on the sediment.

We can also discern the change in the *Rg* shape induced by the changing thickness of the sediment. The duration of the *Rg* phase is gradually increased for longer paths by the influence of seismic dispersion, but is shortened again once the thick sediment is encountered.

5 DISCUSSION AND CONCLUSIONS

The *Lg* phase propagating in the crustal waveguide is normally very prominent at regional distances, but is at the same time very sensitive to substantial lateral variations in crustal structure, especially at continental–oceanic margins.

Sequences of wavefield snapshots and synthetic seismograms calculated by a 2-D anelastic pseudospectral code can provide an improved understanding of the nature of *Lg*-wave propagation in complex media. We have shown using numerical modelling for a single graben model with crustal thinning due to Moho uplift and a sedimentary basin at the surface that there will be severe attenuation for the *Lg* wave and the transmission of mantle *Pn* and *Sn* waves propagating in the uppermost mantle.

We have been able to isolate the influence of different aspects of lateral variation in crustal structure to examine their influence on regional wave propagation. A major contribution to the blockage of *Lg* waves comes from strong scattering induced by the presence of sedimentary basins. Anelastic attenuation in the sediments then helps suppress *S*-wave energy trapped in the sedimentary basin. The change in shape of the crustal waveguide as the crust thins due to Moho uplift helps to reinforce *Lg* attenuation by pushing *S* energy from the crystalline crust into the sediments in the basin. The coherence of the *Lg* phase in simple structures arises from the superposition of multiple *S* reflections within the crust, but the distorted wavefield emerging on the far-side of the crustal barrier is extended by scattering processes and has lost energy by attenuation in the sediments or by leakage into the upper mantle.

We have been able to reproduce the patterns of observations reported by Kennett & Mykkeltveit (1984) for explosion experiments across the central graben of the North Sea using numerical calculations for the seismic wavefield in a realistic 2-D anelastic structure. Even though we were not able to include the thin water layer covering this continental region, we could successfully demonstrate the severe *Lg* attenuation while crossing the graben zone. This attenuation is due to the combination and interaction of a number of factors, including the influence of the geometry of the crustal thinning, attenuation in the sediments and the influence of strong lateral velocity gradients in the model. Although we have considered the regional seismic wavefield by the use of 2-D modelling, further attenuation of the *Lg* phase is expected in the realistic three-dimensionally varying crust due to conversions between *P*, *SV* and *SH* and scattering by 3-D topographical variations of basin and Moho.

The results of the present paper suggest that there is no single mechanism which can provide a simple interpretation of the *Lg*-wave extinction at structures like the North Sea Central Graben. The blockage is not caused just by a thinning crust (Zhang & Lay 1995), strong topographical variations of the Moho (e.g. Bouchon & Coutant 1994), the presence of the overlying water (Cao & Muirhead 1993) or strong intrinsic attenuation by scattering (Campillo *et al.* 1993).

ACKNOWLEDGMENTS

TF would like to acknowledge support from the exchange scheme between the Japan Society for the Promotion of Science

and the Australian Academy of Science for his visit to Canberra. Most of this research was conducted while he was a Visiting Fellow at the Research School of Earth Sciences of the Australian National University.

REFERENCES

- Baumgardt, D.R., 1990. Investigation of teleseismic *Lg* blockage and scattering using regional arrays, *Bull. seism. Soc. Am.*, **80**, 2261–2281.
- Bostock, M.G. & Kennett, B.L.N., 1990. The effect of 3-D structure on *Lg* propagation patterns, *Geophys. J. Int.*, **101**, 355–365.
- Bouchon, M. & Coutant, O., 1994. Calculation of synthetic seismograms in a laterally varying medium by the Boundary Element-Discrete Wavenumber Method, *Bull. seism. Soc. Am.*, **84**, 1869–1881.
- Bowman, R. & Kennett, B.L.N., 1991. Propagation of *Lg* waves in the North Australian craton: influence of crustal velocity gradients, *Bull. seism. Soc. Am.*, **81**, 592–610.
- Campillo, M., 1987. *Lg* wave propagation in laterally varying crust and the distribution of the apparent quality factor in central France, *J. geophys. Res.*, **92**, 12 604–12 614.
- Campillo, M., Feignier, B., Bouchon, M. & Bethoux, N., 1993. Attenuation of crustal waves across the Alpine range, *J. geophys. Res.*, **98**, 1987–1996.
- Cao, S. & Muirhead, K.J., 1993. Finite difference modelling of *Lg* blockage, *Geophys. J. Int.*, **115**, 85–96.
- Cerjan, C., Kosloff, D., Kosloff, R. & Reshef, M., 1985. A nonreflecting boundary condition for discrete acoustic and elastic wave equations, *Geophysics*, **50**, 705–708.
- Furumura, T. & Takenaka, H., 1996. 2.5-D modelling of elastic waves using the pseudospectral method, *Geophys. J. Int.*, **124**, 820–832.
- Gregersen, S., 1984. *Lg*-wave propagation and crustal structure differences near Denmark and the North Sea, *Geophys. J. R. astr. Soc.*, **79**, 217–234.
- Kadinsky-Cade, K., Barazangi, M., Oliver, J. & Isacks, B., 1981. Lateral variations of high-frequency seismic wave propagation at regional distances across the Turkish and Iranian Plateaus, *J. geophys. Res.*, **86**, 9377–9396.
- Kennett, B.L.N., 1986. *Lg* waves and structural boundaries, *Bull. seism. Soc. Am.*, **76**, 1133–1141.
- Kennett, B.L.N. & Mykkeltveit, S., 1984. Guided wave propagation in laterally varying media—II. *Lg*-wave in north western Europe, *Geophys. J. R. astr. Soc.*, **79**, 257–267.
- Kennett, B.L.N., Gregersen, S., Mykkeltveit, S. & Newmark, R., 1985. Mapping of crustal heterogeneity in the North Sea basin via the propagation of *Lg*-waves, *Geophys. J. R. astr. Soc.*, **83**, 299–306.
- Maupin, V., 1989. Numerical modelling of *Lg* wave propagation across the North Sea Central Graben, *Geophys. J. Int.*, **99**, 273–283.
- Ni, J. & Barazangi, M., 1983. High frequency seismic wave propagation beneath the Indian shield, Himalayan Arc, Tibetan Plateau, and surrounding regions: high uppermost mantle velocities and efficient *Sn* propagation beneath Tibet, *Geophys. J. R. astr. Soc.*, **72**, 655–689.
- Nuttli, O., 1980. The excitation and attenuation of seismic crustal phases in Iran, *Bull. seism. Soc. Am.*, **70**, 469–485.
- Pomeroy, P.W., Best, W.J. & McEvelly, T.J., 1982. Test ban treaty verification with regional data—a review, *Bull. seism. Soc. Am.*, **72**, S89–S129.
- Press, F. & Ewing, M., 1952. Two slow surface waves across North America, *Bull. seism. Soc. Am.*, **42**, 219–228.
- Regan, J. & Harkrider, D.G., 1989. Numerical modelling of *SH Lg* waves in and near continental margins, *Geophys. J. Int.*, **98**, 107–130.
- Ruzaikan, A.I., Nersesov, I.L., Khalturin, V.I. & Molnar, P., 1977. Propagation of *Lg* and lateral variation in crustal structure in Asia, *Geophys. J. R. astr. Soc.*, **82**, 307–316.
- Wood, R. & Barton, P., 1983. Crustal thinning and subsidence in the North Sea, *Nature*, **302**, 134–136.
- Zhang, T.-R. & Lay, T., 1995. Why the *Lg* phase does not traverse oceanic crust, *Bull. seism. Soc. Am.*, **85**, 1665–1678.